Supporting Information

A fast micro-nano liquid layer induced construction towards scaled-up oxyhydroxide based electrocatalysts for alkaline water splitting

Yaotian Yan,[#1] Juqing Liu,[#1] Keke Huang,[#1] Junlei Qi,[1] Liang Qiao,[2] Xiaohang Zheng[1] and Wei Cai*[1]*

1. School of Materials Science and Engineering, Harbin Institute of Technology, Harbin, China

2. Key Laboratory of Materials Design and Quantum Simulation, College of Science, Changchun University, Changchun, 130022, China

*Corresponding author. Email: zhengxiaohang@hit.edu.cn (Xiaohang Zheng), weicai@hit.edu.cn (Wei Cai)

[#]These authors contribute equally.

This PDF file includes:

conventional immersion and micro-nano liquid layer induction.

Fig. S14 The phase characterization of other material systems.

Table S1 The standard electrode potentials involved in the manuscript.

Table S2 Thermodynamic data used in the free energy of formation calculations.
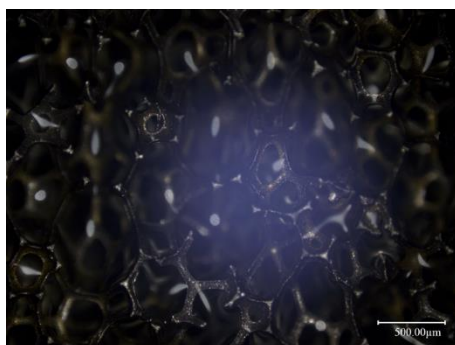
Fig. S1 The digital photo of Ni foam covered by micro-nano liquid layer.
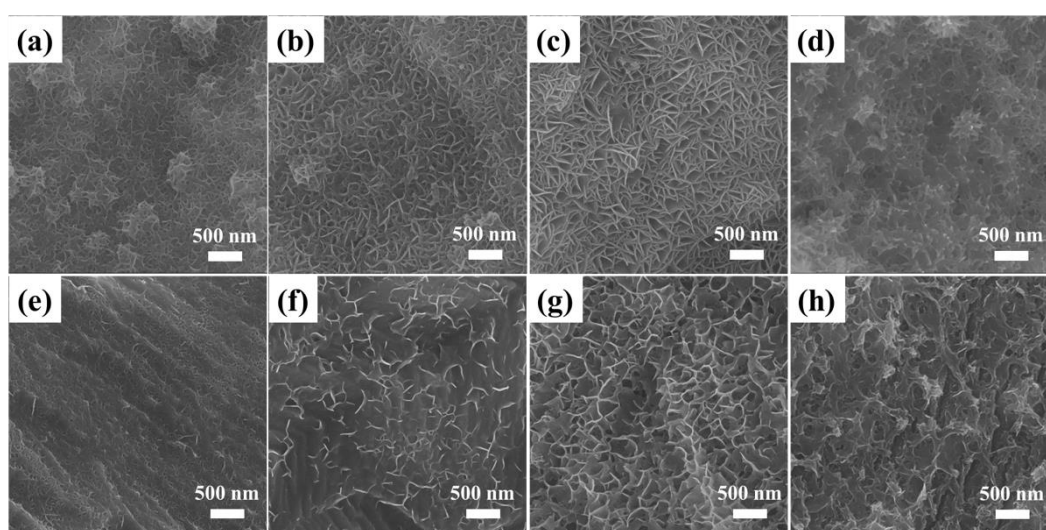

Fig. S2 The influence of concentration and composition ratio of the micro-nano liquid layer on the morphology. The SEM images of (a) Ni-FeOOH-0.018, (b) Ni-FeOOH-0.037, (c) Ni-FeOOH-0.074, (d) Ni-FeOOH-0.148; (e) $Fe_1Ni_xZr_3OOH$, (f) $Fe_2Ni_xZr_2OOH$, (g) $Fe_{2.3}Ni_xZr_{1.7}OOH$, (h) $Fe_3Ni_xZr_1OOH$.

In order to explain the effects of $FeCl_3$ concentrations on morphology and electrocatalytic activities, samples treated by different $FeCl_3$ concentrations (0.018 M, 0.037 M, 0.074 M and 0.148M) were also prepared, marked as Ni-FeOOH-0.018, Ni-FeOOH-0.037, Ni-FeOOH-0.074, Ni-FeOOH-0.148 respectively.

Based on the optimal Fe cation concentration, the samples treated by ionic solutions with different $FeCl_3/ZrCl_4$ ratios ($FeCl_3$: $ZrCl_4$= 1: 3, 2: 2, 2.3: 1.7, 3: 1, and the total concentration remained unchanged at 0.13 M) were also prepared to illustrate the effects of composition, marked as $Fe_1Ni_xZr_3OOH$, $Fe_2Ni_xZr_2OOH$, $Fe_{2.3}Ni_xZr_{1.7}OOH$, $Fe_3Ni_xZr_1OOH$ respectively.
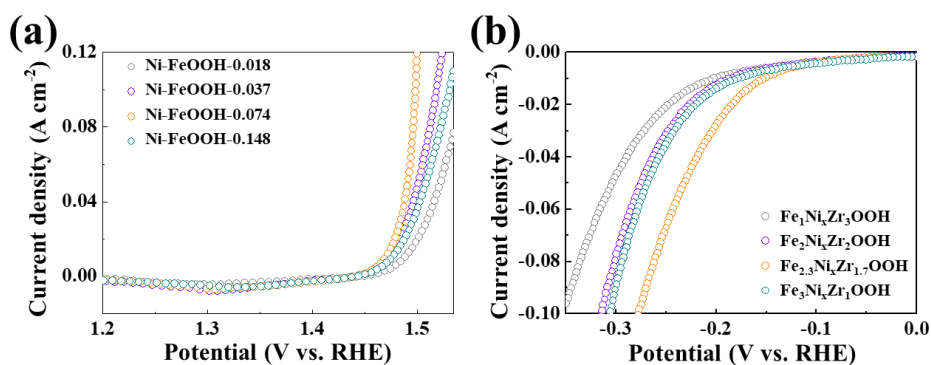
Fig. S3 Performance tests of samples prepared with different technological parameters. (a) The OER polarization curves of different Ni-FeOOH samples prepared with $FeCl_3$ solutions of different concentration; (b) the HER polarization curves of different ZrNi-FeOOH samples prepared with $FeCl_3/ZrCl_4$ solutions of different ratios.
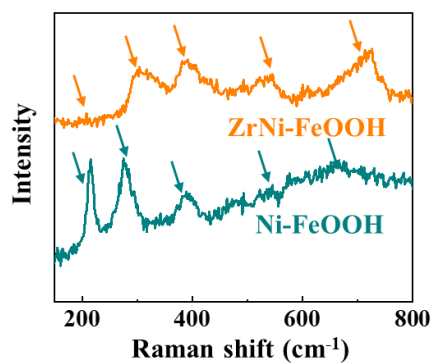

Fig. S4 The Raman spectra of as prepared samples.

It should be noted that while after Zr incorporation, the signals were consistent but slightly different. The peak intensity at ~200 cm^{-1} is greatly reduced, while the peak intensity at ~537 cm^{-1} and ~722 cm^{-1} is strengthened, indicating the effect of Zr atoms on the lattice.
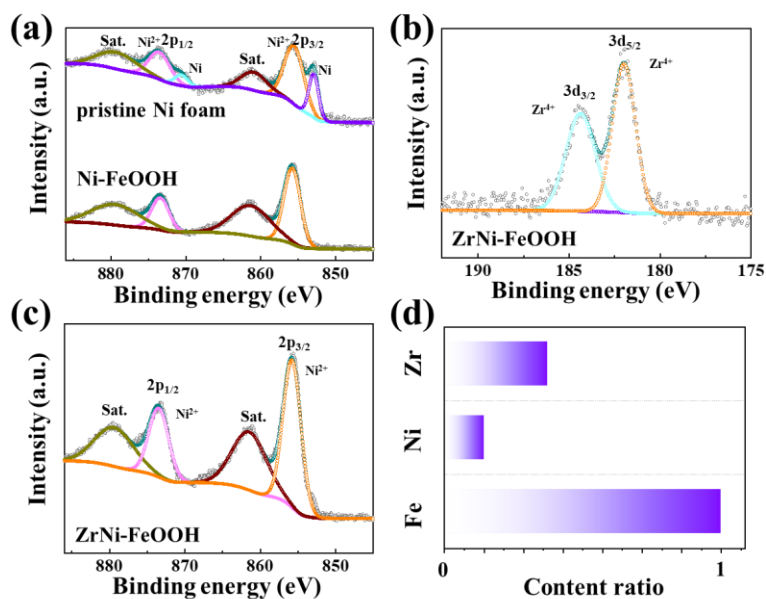
Fig. S5 Chemical states of the main samples. The XPS spectra of (a) Ni 2p of pristine Ni foam and Ni-FeOOH; (b) Zr 3d of Zr, Ni-FeOOH; (c) Ni 2p of Zr, Ni-FeOOH. (d) The content ratio of cations components standardized by atomic percentage of Fe.
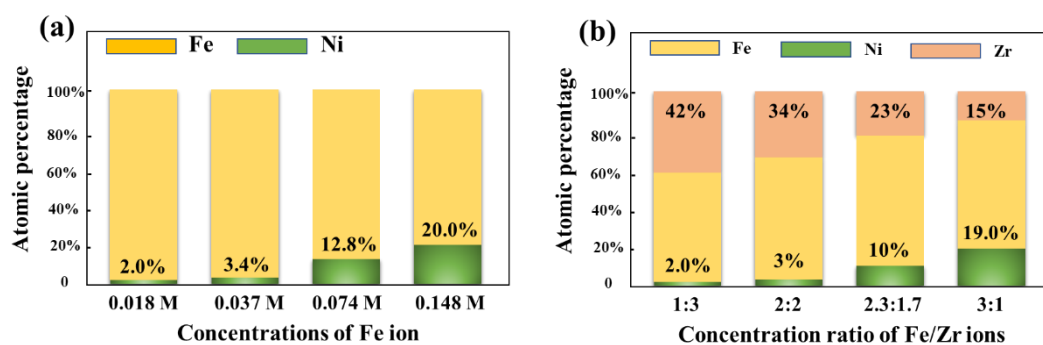
Fig. S6 Inductively coupled plasma-optical emission spectroscopy (ICP-OES) results. (a) Ni-FeOOH samples and (b) ZrNi-FeOOH samples generated by different ion concentrations. It should be noted that the total concentration of Fe and Zr ions remains unchanged at 0.13 M for (b).

Fig. S7 The stability of ZrNi-FeOOH nanosheet. The chronopotential analysis curves of (a) OER, (b) HER and (c) overall water splitting.

Fig. S8 The water splitting device driven by Stirling engine.
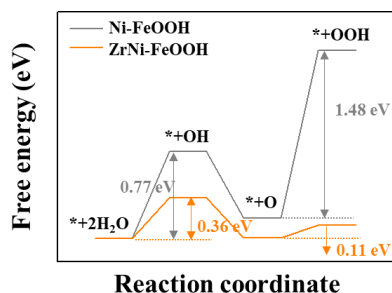
Fig. S9 The DFT calculations of intermediates adsorption energy for OER. The free energy diagram of *OH, *O and *OOH adsorption on Fe site of Ni-FeOOH and ZrNi-FeOOH in OER process.
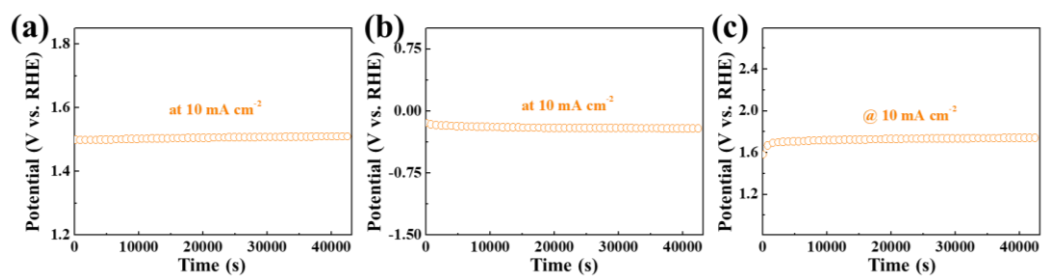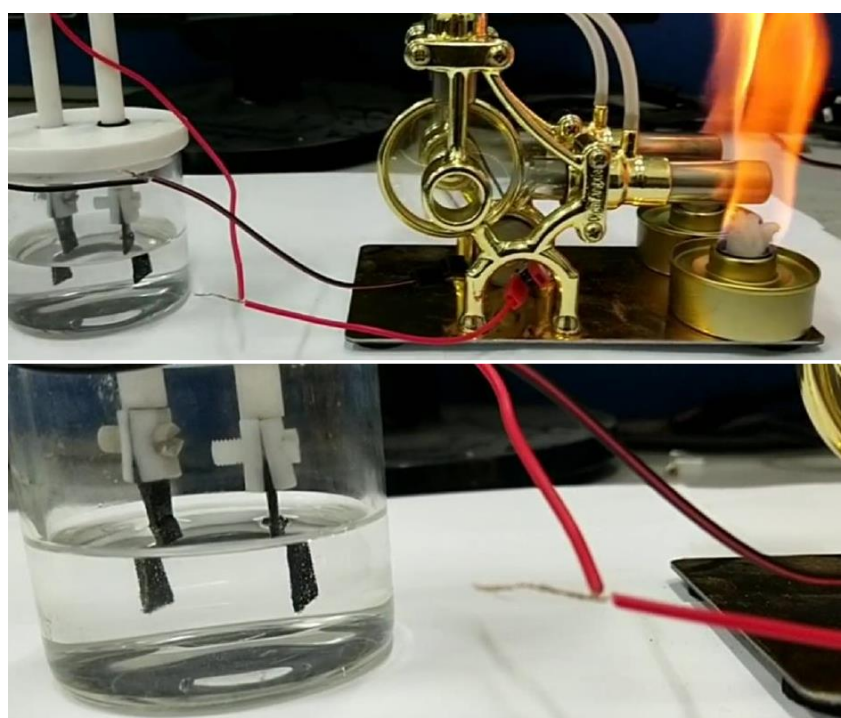
The free energy was calculated using the equation:

$G = E + ZPE - TS$

where G, E, ZPE and TS are the free energy, total energy, zero-point energy and entropic contributions (T was 298.15K) from DFT calculations, respectively. The G values for calculations are shown in **Table S1**.

The OER process would go through the following steps in sequence:

$* + 2H_2O \rightarrow *OH + H_2O + H^+ + e^-$;

$*OH \rightarrow *O + H^+ + e^-$;

$*O + H_2O \rightarrow *OOH + H^+ + e^-$;
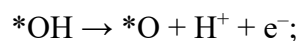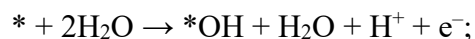
where making G(* + 2H$_2$O) the zero point, the free energy diagram is drawn according to the principle of atoms conservation.

Fig. S10 The Fe 2p signals of powder XPS spectra of Ni-FeOOH and ZrNi-FeOOH.

For the XPS spectra, the sensitivity factor and detection limit of the main peak of different elements are different. Besides, the Fe element owns a strong magnetic, having obvious effect on photoelectron overflow. Thus, the XPS spec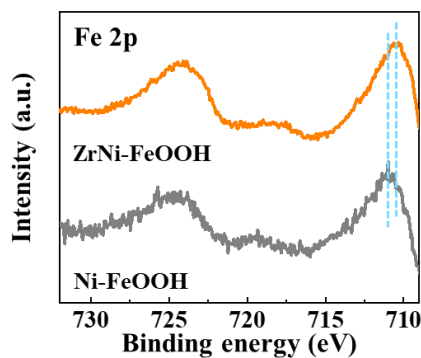trum of Fe element usually owns more obvious noises than other elements, which also has been observed by previous researches. Since that the nanostructure is in-situ generated on the surface of Ni-foam, the total amount of active substances detected is very small, which also exacerbates Fe signal noise. To dispel this doubt, the XPS analysis of as collected powder is conducted to improve signal-to-noise ratio of Fe 2p signal. It should be noted that the ZrNi-FeOOH sample owns similar negative shift towards low binding energy to that in the manuscript, which supports related discussions of the manuscript.

Fig. S11 The determination of corrosion potential and corrosion current for evaluating the formation of Ni-FeOOH nanosheet. The calculation of i_{corr} and E_{corr} of Ni foam substrate in (a) NaCl, (b) $FeCl_3$, (c) $Fe(NO_3)_3$ and (d) $Fe_2(SO_4)_3$ solutions with concentrations standardized according to the optimal $FeCl_3$ concentration.

To conduct the polarization curves tests, the optimal concentration of $FeCl_3$ solution (0.074 M) is taken as benchmark. Thus, the concentrations of NaCl, $Fe(NO_3)_3$ and $Fe_2(SO_4)_3$ are 0.222 M, 0.074 M and 0.037 M respectively.
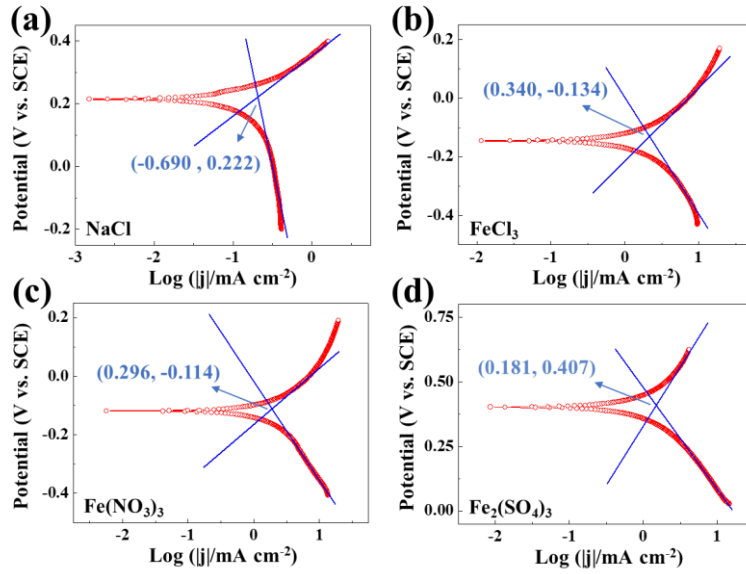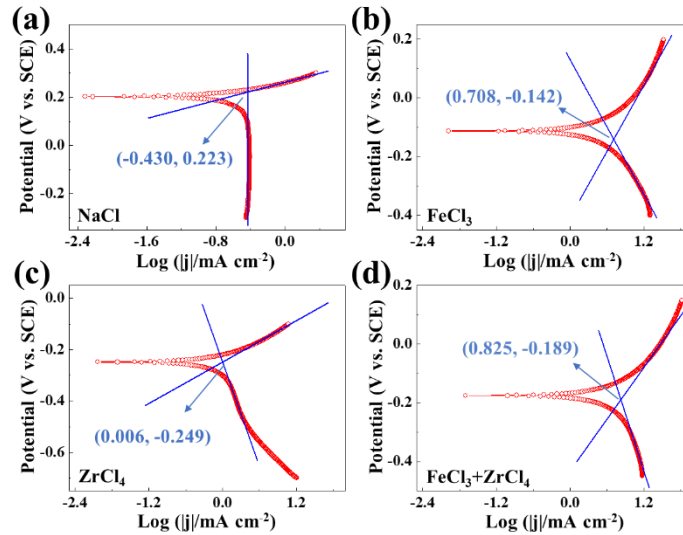
Fig. S12 The determination of corrosion potential and corrosion current for evaluating the formation of ZrNi-FeOOH nanosheet. The calculation of i_{corr} and E_{corr} of Ni foam substrate in (a) NaCl, (b) $FeCl_3$, (c) $ZrCl_4$ and (d) $FeCl_3/ZrCl_4$ solutions with concentrations standardized according to the optimal Fe/Zr ratio.

To conduct the polarization curves tests, the optimal concentration of $FeCl_3/ZrCl_4$ mixed solution (0.13 M) is taken as benchmark, which contains 0.074 M $FeCl_3$ and 0.056 M $ZrCl_4$. Thus, the concentrations of NaCl, $FeCl_3$ and $ZrCl_4$ are all 0.13 M.
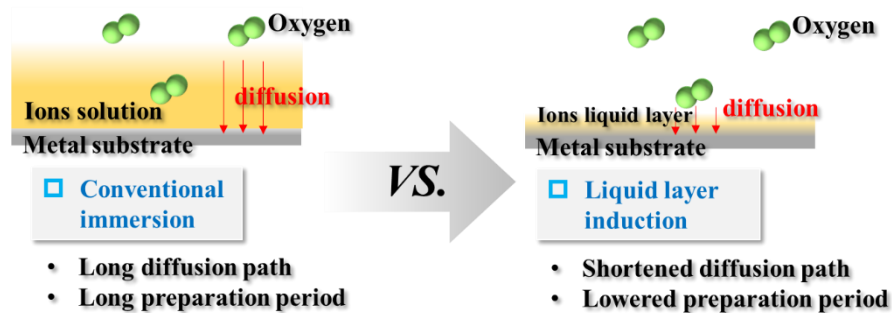

Fig. S13 The illustration of the comparison between different corrosion strategies of conventional immersion and micro-nano liquid layer induction.
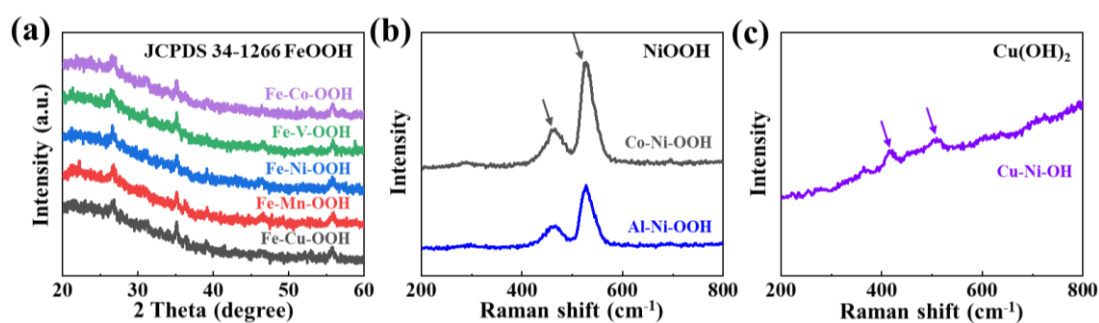
Fig. S14 The phase characterization of other material systems. (a) The XRD patterns of Fe-Co, Fe-V, Fe-Ni, Fe-Mn and Fe-Cu systems; (b) the Raman spectra of Co-Ni and Al-Ni systems; (c) the Raman spectra of Cu-Ni system.

It can be seen that the products of Fe-contained binary cation systems own a crystal nature of FeOOH, which is consistent with the main case studies of the manuscript. The Raman spectra of Co-Ni and Al-Ni systems suggest peaks at ~455 and 535 cm^{-1}, which is attributed to the Ni^{III}-O bands in NiOOH. While for Cu-Ni system, the Raman peaks at ~418 and ~512 cm^{-1} correspond to O-Cu-O stretch modes in Cu(OH)$_2$ phase. It can be concluded that the dominant element of product phase depends on the standard electrode potential. From the phase characterization results of our manuscript, it is found that the higher the electrode potential, the more favorable the element becomes dominant. For instance, compared with Co^{2+} (ψ = -0.277 V), V^{3+} (ψ = 0.337 V), Ni^{2+} (ψ = -0.246 V), Mn^{2+} (ψ = -1.182 V) and Cu^{2+} (ψ = 0.337 V), the Fe^{3+} (ψ = 0.771 V) owns much higher standard electrode potential, while the relevant systems own the product phase of FeOOH. Besides, compared with Co^{2+} (ψ = -0.277 V) and Al^{3+} (ψ = -1.66 V), the Ni^{2+} (ψ = -0.246 V) owns higher standard electrode potential, while the relevant systems own the product phase of NiOOH. Compared with Ni^{2+} (ψ = -0.246 V), the Cu^{2+} (ψ = 0.337 V) owns much higher standard electrode potential, while the relevant systems own the product phase of Cu(OH)$_2$. These further prove that the ions with higher standard electrode potential own higher thermodynamic trends to bond negatively charged species (OH$^-$, OOH$^-$ *etc.*), therefore becoming the dominant species.

Table S1 The standard electrode potentials involved in the manuscript

Half reaction	Standard electrode potential (ψ/V)
$O_2 + 2H_2O + 4e^- \rightarrow 4OH^-$	~0.806
$Co^{2+} + 2e^- \rightarrow Co$	-0.277
$VO_2^+ + 2H^+ + 2e^- \rightarrow V^{3+} + H_2O$	0.337
$Ni^{2+} + 2e^- \rightarrow Ni$	-0.246
$Mn^{2+} + 2e^- \rightarrow Mn$	-1.182
$Cu^{2+} + 2e^- \rightarrow Cu$	0.337
$Al^{3+} + 3e^- \rightarrow Al$	-1.66
$Fe^{3+} + e^- \rightarrow Fe^{2+}$	0.771
$Fe^{2+} + 2e^- \rightarrow Fe$	-0.447

Table S2 Thermodynamic data used in the free energy calculations.

	G (eV)
H_2O	-11.51
H_2	-4.92
O_2	-8.27
Ni-FeOOH-interstice	-33568.31
Ni-FeOOH-replacement	-30123.55
ZrNi-FeOOH-interstice	-38749.00
ZrNi-FeOOH-replacement	-35317.04